An Absolute Asymmetric Synthesis of the [2 + 2] Cycloadduct via Single Crystal-to-Single Crystal Transformation by Charge-Transfer Excitation of Solid-State Molecular Complexes Composed of Arylolefins and Bis[1,2,5]thiadiazolotetracyanoquinodimethane†

Takanori Suzuki,[1a] Takanori Fukushima,[1a] Yoshiro Yamashita,[1b] and Tsutomu Miyashi*,[1a]

Contribution from the Department of Chemistry, Faculty of Science, Tohoku University, Aramaki, Sendai 980, Japan, and Institute for Molecular Science, Okazaki 444, Japan

Received November 1, 1993•

Abstract: The title electron acceptor, bis[1,2,5]thiadiazolotetracyanoquinodimethane (BTDA, **1**), formed weak electron-donor–acceptor (EDA) complexes with arylolefins such as styrene (ST) and divinylbenzenes (DVs). Upon charge-transfer (CT) excitation of these complexes in MeCN, the [2 + 2]-type cycloadducts (**2**) were formed via a single electron transfer. Similar cycloaddition reactions were efficiently induced when the solid-state molecular complexes of **1** and arylolefins were irradiated. In contrast to the close similarities in solution photochemistry, the solid-state reactivities of three isomeric divinylbenzenes (*o*DV, *m*DV, *p*DV) were quite dissimilar because of the different molecular overlaps of **1** and DVs in the crystal. The apparent reactivity of the *o*DV·**1** crystal was much higher than that in solution as in the case of the ST·**1** crystal, and adduct **2o** was formed via the single crystal-to-single crystal transformation. Because of the asymmetric crystal structure in *o*DV·**1**, the optically pure product with 95% ee was obtained from the achiral components without any external chiral source. On the other hand, the incomplete conversion of the *m*DV·**1** crystal to **2m** is due to the crystal-to-amorphous transformation, and the 1:2 adduct **6** was formed on irradiation of the *p*DV·**1** crystal which could not be obtained on excitation of the EDA complex in MeCN.

The physical properties of molecular complexes attract much attention in the field of materials chemistry, and a large number of charge-transfer (CT) crystals have been thoroughly investigated due to their intriguing behaviors such as electrical conduction[2] and ferromagnetism.[3] However, few studies have so far been made on their photoreactivities in the crystal. It is well-known that the photoexcitations of weak CT pairs in solution afford radical ion pairs by a single electron transfer (ET),[4] so that the photoirradiations of the CT crystals will provide a unique opportunity to investigate the reactions of radical ions included in the highly organized crystal lattices. Because these reactions would exhibit the intriguing behavior characteristic to both the photoinduced electron-transfer (PET) reactions and the organic solid-state reactions, photochemistry of CT crystals can serve as a new motif to be exploited.[5] The PET process seems more advantageous in CT crystals than in solution because of the preorganized face-to-face overlap of the donor and the acceptor in the crystal. Furthermore, for chemical reactions followed by ET, the high regio- and stereoselectivities are expected because reaction pathways will be confined by "topochemical control",[6] which was well demonstrated in the research of [2 + 2] cycloadditions of olefins in the excited state.[7-10]

In the field of the organic solid-state reactions, special attention has been focused recently on the "absolute" asymmetric synthesis[7,11] by using the spontaneous asymmetric crystallization of achiral compounds coupled with their topochemical transformation giving the chiral products. For the successful execution of such an asymmetric synthesis, "engineering"[12] of the substrate crystal is of significant importance which allows the prediction and designing of molecular arrangements. It has been reported that weakly attractive C–H--O and Cl--Cl interactions are useful for the crystal engineering because of their directional preferences.[13] Furthermore, the intermolecular interaction in the crystal was suggested to take an important part in maintaining the

† Dedicated to Prof. Toshio Mukai on the occasion of his 70th birthday.

• Abstract published in *Advance ACS Abstracts,* March 1, 1994.

(1) (a) Tohoku University. (b) Institute for Molecular Science.

(2) Bechgaard, K. In *Structure and Properties of Molecular Crystals: Organic Conductors*; Pierrot, M., Ed.; Elsevier: Amsterdam, 1990; pp 235–295 and references cited therein.

(3) Miller, J. S.; Epstein, A. J.; Reiff, W. M. *Chem. Rev.* **1988**, *88*, 201. Kollmac, C.; Kahn, O. *Acc. Chem. Res.* **1993**, *26*, 259 and references cited therein.

(4) Foster, R. In *Organic Charge-Transfer Complex*; Academic Press: London and New York, 1969; pp 303–334.

(5) Recently the photodimerization reactions were studied on the CT crystals of cinnamic acids having the electron-donating and -accepting substituents although the CT excited state (radical ion pair) was not considered to be conducive to photoreactivity: Sarma, J. A. R. P.; Desiraju, G. R. *J. Chem. Soc., Perkin Trans. 2* **1985**, 1905. Desiraju, G. R.; Sharma, C. V. K. M. *J. Chem. Soc., Chem. Commun.* **1991**, 1239.

(6) Cohen, M. D.; Schmidt, G. M. J. *J. Chem. Soc.* **1964**, 1996. Cohen, M. D.; Schmidt, G. M. J.; Sonntag, F. I. *J. Chem. Soc.* **1964**, 2000. Schmidt, G. M. J. *J. Chem. Soc.* **1964**, 2014.

(7) Perrin, R.; Lamartine, R. In *Structure and Properties of Molecular Crystals: Organic Reactions in the Solid State*; Pierrot, M., Ed.; Elsevier: Amsterdam, 1990; pp 107–159 and references cited therein.

(8) Other representative examples of topochemical control include the polymerization of several diacetylene derivatives (ref 9) as well as the [2 + 2] photopolymerization of distyrylpyrazine derivatives (ref 10).

(9) Wegner, G. *Z. Naturforsh. B* **1969**, *24*, 824. Baughman, R. H. *J. Appl. Phys.* **1972**, *43*, 4362. Baughman, R. H. *J. Chem. Phys.* **1978**, *68*, 3110.

(10) Iguchi, M.; Nakanishi, H.; Hasegawa, M. *J. Polym. Sci., Part A-1* **1968**, *6*, 1055. Nakanishi, H.; Jones, W.; Thomas, J. M.; Hasegawa, M.; Rees, W. L. *Proc. R. Soc. London, Ser. A* **1980**, *369*, 307. Hasegawa, M.; Kinbara, K.; Adegawa, Y.; Saigo, K. *J. Am. Chem. Soc.* **1993**, *115*, 3820.

(11) Addadi, L.; van Mil, J.; Lahav, M. *J. Am. Chem. Soc.* **1982**, *104*, 3422. Evans, S. V.; Garcia-Garibay, M.; Omkaram, N.; Scheffer, J. R.; Trotter, J.; Wireko, F. *J. Am. Chem. Soc.* **1986**, *108*, 5648. Hasegawa, M.; Chung, C.-M.; Muro, N.; Maekawa, Y. *J. Am. Chem. Soc.* **1990**, *112*, 5676. Sakamoto, M.; Hokari, N.; Takahashi, M.; Fujita, T.; Watanabe, S.; Iida, I.; Nishio, T. *J. Am. Chem. Soc.* **1993**, *115*, 818. Kaupp, G.; Haak, M. *Angew. Chem., Int. Ed. Engl.* **1993**, *32*, 694. Roughton, A. L.; Muneer, M.; Demuth, M.; Klopp, I.; Krüger, C. *J. Am. Chem. Soc.* **1993**, *115*, 2085.

(12) Desiraju, G. R. *Crystal Engineering: The Design of Organic Solid*; Elsevier: Amsterdam, 1989.

(13) Sarma, J. A. R. P.; Desiraju, G. R. *Acc. Chem. Res.* **1986**, *19*, 222. Recently, the weak interactions through the Cl--N≡C and C-H--N contacts were reported also effective in regulating the molecular arrangements in the crystal: Reddy, D. S.; Panneerselvam, K.; Pilati, T.; Desiraju, G. R. *J. Chem. Soc., Chem. Commun.* **1993**, 661. Reddy, D. S.; Goud, B, S.; Panneerselvam, K.; Desiraju, G. R. *J. Chem. Soc., Chem. Commun.* **1993**, 663.

0002-7863/94/1516-2793$04.50/0

topotaxy during the course of the solid-state reaction.[14] In the case of topotactic reactions, the detailed reaction sequence can be visualized by means of X-ray structural analyses of both the reactant and the product,[15] which facilitates the better understanding of chemical reactions.

In this connection, the title electron acceptor, bis[1,2,5]-thiadiazolotetracyanoquinodimethane (BTDA, **1**), is of interest

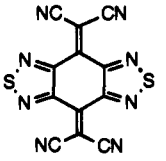

BTDA **1**

ST : R = H
oDV : R = 2-vinyl
mDV: R = 3-vinyl
pDV : R = 4-vinyl

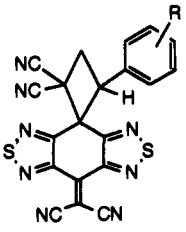

2st : R = H
2o : R = 2-vinyl
2m : R = 3-vinyl
2p : R = 4-vinyl

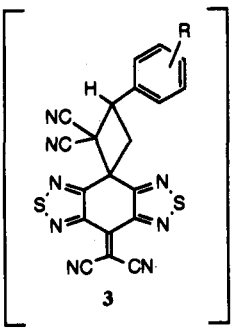

3

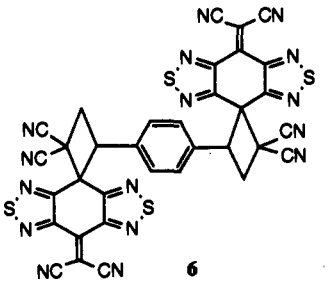

6

in which the novel interaction between sulfur atoms and cyano groups was discovered. This interaction is also one of the sources of directionality in determining the crystal packing of organic molecules and stabilizes the crystalline state by electrostatic factors.[16] Furthermore, **1** formed inclusion cavities by this interaction in its CT crystals with aromatic hydrocarbons, resulting in the separation of isomeric disubstituted benzenes by selective complexation with **1**.[16] These findings prompt us to explore the CT excitation reactions of the solid-state molecular complexes of **1** in the anticipation that the unique reaction cavities for the hydrocarbon donors will be provided by the S--N≡Cinteraction of **1**.

Arylolefins are suitable electron donors in this work because of the sufficient donating properties of the benzene nuclei as well as the versatile reactivities at the vinyl groups in their cation radicals.[17] We have chosen styrene (ST), the simplest arylolefin, as well as three isomers of bifunctional divinylbenzenes (*o*DV, *m*DV, *p*DV).[18] It has been found that all of them form weak electron-donor–acceptor (EDA) complexes with **1** (E^{red}, –0.02 V) and also that these complexes can be isolated as stable CT crystals. We report here the [2 + 2]-type cycloaddition reactions of **1** with arylolefins, which were induced by the CT excitation in the solid state. The reactivities of CT crystals were quite different from those of EDA complexes in solution, and the variety in the solid-state reactivities of DV isomers could be accounted for by the different molecular arrangement of **1** and DV in the crystal. It is worth noting that the absolute asymmetric synthesis could be realized on irradiation of the *o*DV·**1** CT crystal giving the chiral adduct (**2o**) with high optical purity (95% ee). This reaction made a new entry into the rare examples of the single crystal-to-single crystal transformation.[19] A plausible mechanism is also discussed for the temperature dependence of the optical yield of **2o**.

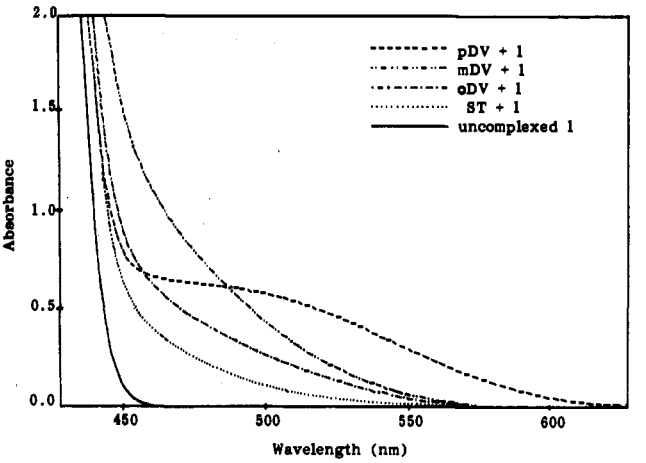

Figure 1. CT absorption spectra of the EDA complexes of **1** with arylolefins in MeCN ([arylolefin] = 5.0×10^{-2} mol dm^{-3} and [**1**] = 1.0×10^{-2} mol dm^{-3}).

Table 1. Oxidation Potentials (E_{ox})[a] of Donors, Association Constants (K_{CT})[b] for EDA Complexes, and CT Excitation Reactions of EDA Complexes in MeCN[c] and of CT Crystals in the Solid State[d]

			EDA complexes		CT crystals
donor	E_{ox} (V)	K_{CT} (dm^3 mol^{-1})	product yield[e] (%)	recovery of **1**[e] (%)	product yield (%)
*p*DV	+1.51	1.5	**2p**, 8	67	**2p**, 8;[f] **6**, 2[f]
*m*DV	+1.83	1.4	**2m**, 11	50	**2m**, 15[f]
*o*DV	+1.82	1.1	**2o**, 9	63	**2o**, 91[e]
ST	+1.90	0.85	**2st**, 4	78	**2st**, 71[e,g]

[a] *E* (V vs SCE) measured in MeCN containing 0.1 mol dm^{-3} of Et_4NClO_4 as a supporting electrolyte; Pt wire, scan rate of 100 mV s^{-1}. [b] Measured at 20 °C in MeCN. [c] A 10-mL MeCN solution was irradiated with a 2-kW Xe lamp for 5 h at 20 °C; $\lambda > 450$ nm, [**1**] = 1.0×10^{-2} mol dm^{-3}, [donor] = 5.0×10^{-3} mol dm^{-3}. [d] A 10-mL water suspension of the CT crystal (1.0×10^{-4} mol) was irradiated with a 2-kW Xe lamp for 1 h at 15 °C, $\lambda > 540$ nm. [e] Isolated yields. [f] Determined on the basis of ^{1}H NMR spectra. [g] $\lambda > 505$ nm.

Results and Discussion

Cycloaddition of Arylolefins and BTDA (1) via Photoexcitation of EDA Complexes in Solution. Figure 1 shows the absorption spectra of the EDA complexes obtained upon admixing a yellow solution of **1** in MeCN with colorless ST or DV isomers separately. The absorptions in the 450–600-nm region were assigned to the CT bands from HOMOs of arylolefins to the LUMO of **1** because **1** has no significant absorption above 450 nm. The association constants (K_{CT}) were determined by the spectrophotometric procedure at 20 °C in MeCN (Table 1). These small values

(14) Nakanishi, H.; Jones, W.; Thomas, J. M.; Hursthouse, M. B.; Motevalli, M. *J. Phys. Chem.* **1981**, *85*, 3636.
(15) Ohashi, Y. *Acc. Chem. Res.* **1988**, *21*, 268 and references cited therein.
(16) Suzuki, T.; Fujii, H.; Yamashita, Y.; Kabuto, C.; Tanaka, S.; Harasawa, M.; Mukai, T.; Miyashi. T. *J. Am. Chem. Soc.* **1992**, *114*, 3034.
(17) Miyashi, T.; Ikeda, H.; Konno, A.; Okitsu, O.; Takahashi, Y. *Pure Appl. Chem.* **1990**, *62*, 1531.
(18) Recently the [2 + 2] and [4 + 2] cycloadditions of *m*DV and *p*DV with tetracyanoethylene were reported to occur at 28 °C in the dark. Padias, A. B.; Tien, T.-P.; Hall, H. K., Jr. *J. Org. Chem.* **1991**, *56*, 5540.
(19) Nakanishi, H.; Hasegawa, M.; Sasada, Y. *J. Polym. Sci., Polym. Phys. Ed.* **1977**, *15*, 173. Enkelmann, V.; Leyrer, R. J.; Schleier, G.; Wegner, G. *J. Mater. Sci.* **1980**, *15*, 168. Miller, E. J.; Brill, T. B.; Rheingold, A. L.; Fultz, W. C. *J. Am. Chem. Soc.* **1983**, *105*, 7580. Chang, H. C.; Popovitz-Biro, R.; Lahav, M.; Leiserowitz, L. *J. Am. Chem. Soc.* **1987**, *109*, 3883. Wang, W.-N.; Jones, W. *Tetrahedron* **1987**, *43*, 1273.

Table 2. Details of X-ray Structural Analyses

	*o*DV·**1**	chiral-**2o**	*dl*-**2o**	*m*DV·**1**	*p*DV·**1**
formula	$C_{22}H_{10}N_8S_2$	$C_{22}H_{10}N_8S_2$	$C_{22}H_{10}N_8S_2$	$C_{22}H_{10}N_8S_2$	$C_{22}H_{10}N_8S_2$
fw	450.50	450.50	450.50	450.50	450.50
space group	$P2_1$	$P2_1$	$P2_1/n$	$P\bar{1}$	$P\bar{1}$
a (Å)	8.866(2)	9.120(1)	14.759(1)	9.238(4)	8.882(4)
b (Å)	16.764(3)	16.394(2)	9.659(1)	17.264(6)	9.418(4)
c (Å)	7.006(3)	7.181(1)	15.120(1)	7.046(5)	7.363(3)
α (deg)	90.0	90.0	90.0	94.21(4)	108.96(3)
β (deg)	99.63(2)	106.27(1)	106.00(1)	104.65(4)	95.14(4)
γ (deg)	90.0	90.0	90.0	103.93(3)	111.91(3)
V (Å^3)	1026.6(5)	1030.7(3)	2071.9(3)	1044.4(9)	524.6(4)
Z	2	2	4	2	1
ρ_{calcd} (g cm^{-3})	1.457	1.452	1.444	1.433	1.426
cryst dimens (mm)	0.30 × 0.15 × 0.15	0.20 × 0.15 × 0.05	0.20 × 0.20 × 0.15	0.30 × 0.10 × 0.10	0.20 × 0.10 × 0.05
absorp coeff (cm^{-1})	2.743	2.742	2.728	2.706	2.693
$2\theta_{max}$ (deg)	55	50	55	52	52
no. of total data measd	2483	1886	4945	4035	2251
no. of obsd unique data	1950 (3σ)	1214 (3σ)	4315 (non-zero)	2045 (3σ)	1591 (3σ)
residual electron density (e/Å^3)	0.20	0.58	0.43	0.45	0.52
no. of params	330	290	330	330	164
R (%)	4.22	8.21	7.72	8.34	6.62

indicate the presence of only weak CT interactions between arylolefins and **1** in the ground-state EDA complexes.

It seems desirable to examine the photoreactions of **1** with arylolefins in solution before investigating the solid-state reactivities of CT crystals. In order to excite the CT bands selectively, the output from a 2-kW xenon lamp passed through a glass cut filter was used (cutoff $\lambda < 450$ nm). When a 10-mL solution of **1** (1.0×10^{-2} mol dm^{-3}) and *p*DV (5.0×10^{-2} mol dm^{-3}) in MeCN[20] was irradiated for 5 h at 20 °C, the [2 + 2]-type cycloaddition occurred between *p*DV and **1** to give **2p** as a sole product in 8% yield. The yield of **2p** was raised up to 44% upon prolonged irradiation (20 h), but the reaction mixture became rather complicated and contained many undefinable products. Similar irradiation of the EDA complex of **1** with *m*DV, *o*DV, or ST for 5 h in MeCN gave adducts **2m** (11%), **2o** (9%), and **2st** (4%), respectively (Table 1). The regiochemistry of **2o** was determined by the X-ray analysis (Table 2), those of **2p**, **2m**, and **2st** were deduced from the similarity of ^{1}H NMR spectra to that of **2o**, and their regioisomers **3** could not be detected in the reaction mixtures.

Because the local excited state (^{1}**1***) could not be attained by the above irradiation conditions, these reactions proceed via radical ion pairs formed by ET from arylolefins to **1** as shown in Scheme 1. The stepwise bond making of radical ions is favorable for the formation of **2** because of the large stabilization of zwitterions **4** or the corresponding diradicals by resonance. The absence of **3** in the reaction mixtures can be accounted for by considering that the hypothetical intermediate **5** (or **5'**) is less stable than **4**. Anyway, despite the number of vinyl groups or their substituting positions in the benzene nucleus, the EDA complexes reacted similarly on irradiation in MeCN. On the other hand, solid-state reactivities were quite different from those in solution and were largely changed for the isomeric DV·**1** CT crystals as described in the next section.

Preparation of CT Crystals and Their Photoreactivities in the Solid State. Recrystallization of **1** from MeCN containing *p*DV in excess afforded the *p*DV**1** (1:1) CT crystal as purple plates. The CT crystals of *m*DV·**1** (1:1) and *o*DV·**1** (1:1) were obtained as reddish powders by admixing **1** with neat mDV or *o*DV, respectively.[21] In spite of the weaker donating property of ST than DVs, the ST·**1** (1:1) crystal was successfully isolated as an orange powder by the similar direct method. On exposure to any organic solvents, *o*DV·**1** and ST·**1** dissociated into **1** and donors

(20) The low solubility of **1** prevented the usage of other organic solvents (e.g. CH_2Cl_2) for the CT excitation reactions of the EDA complexes; the concentration of the saturated solution of **1** in CH_2Cl_2 is ca. 3×10^{-3} mol dm^{-3} at 40 °C.

Scheme 1

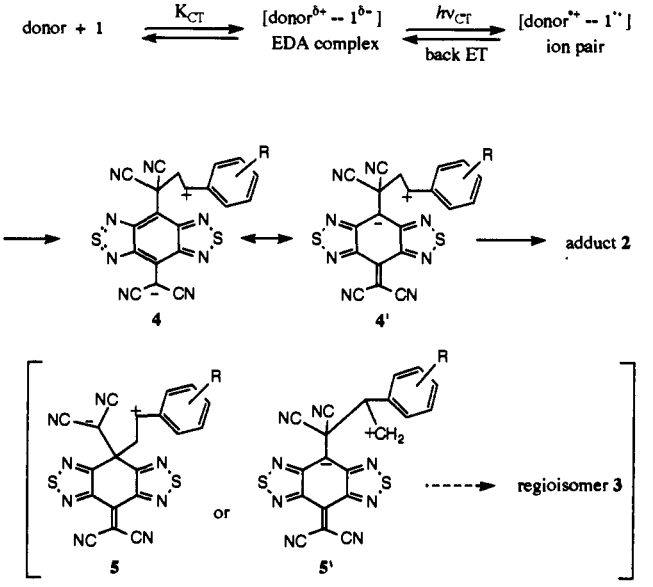

so easily that water suspensions were irradiated at 15 °C throughout the solid-state reactions unless indicated otherwise.

Upon irradiation of a fine powder of ST·**1**, the regiospecific cycloaddition occurred smoothly, and adduct **2st** was obtained as a sole product. The apparent reactivity in the solid state is much higher than that in solution because **2st** was obtained in high yield (71%) within a shorter irradiation period (1 h) with longer wavelength light ($\lambda > 505$ nm). In the case of *o*DV·**1**, the photoreactivity is much more prominent; the adduct **2o** was isolated in 84% yield on irradiation for 15 min with much lower energy light ($\lambda > 540$ nm), and the yield was raised up to 91% by 1 h of irradiation. These results clearly show that the cycloaddition via ET actually occurs even in the solid state by the

(21) In the case of *m*DV, complexations with **1** were found to afford two phases of CT crystals depending on the crystallization conditions. Rapid complexation by the direct method gave the 1:1 complex (phase A, *m*DV·**1**) as a reddish powder, whereas by the slow cooling method or vapor diffusion method, the 5:3 complex (phase B, mDV$_5$·**1**$_3$) was also obtained as orange plates accompanied with red needles of phase A. These crystals could be separated by hand under a microscope. The X-ray analysis of phase B revealed the presence of one-dimensional mixed stacks of *m*DV and **1**, but the "ribbon" network of **1** was absent in this crystal because of the intercalation of *m*DV molecules between the coplanar arrangement of **1**. Crystal data for mDV$_5$·**1**$_3$: $C_{86}H_{50}N_{24}S_6$, fw 1611.86, space group $P\bar{1}$, a = 12.422(4) Å, b = 15.141(3) Å, c = 11.840(5) Å, α = 97.72(3)°, β = 116.19(2)°, γ = 88.24(3)°, V = 1979.2(12) Å^3, Z = 1, ρ_{calcd} = 1.352 g cm^{-3}, R = 9.40%. Details of the crystal structure are given in the supplementary material.

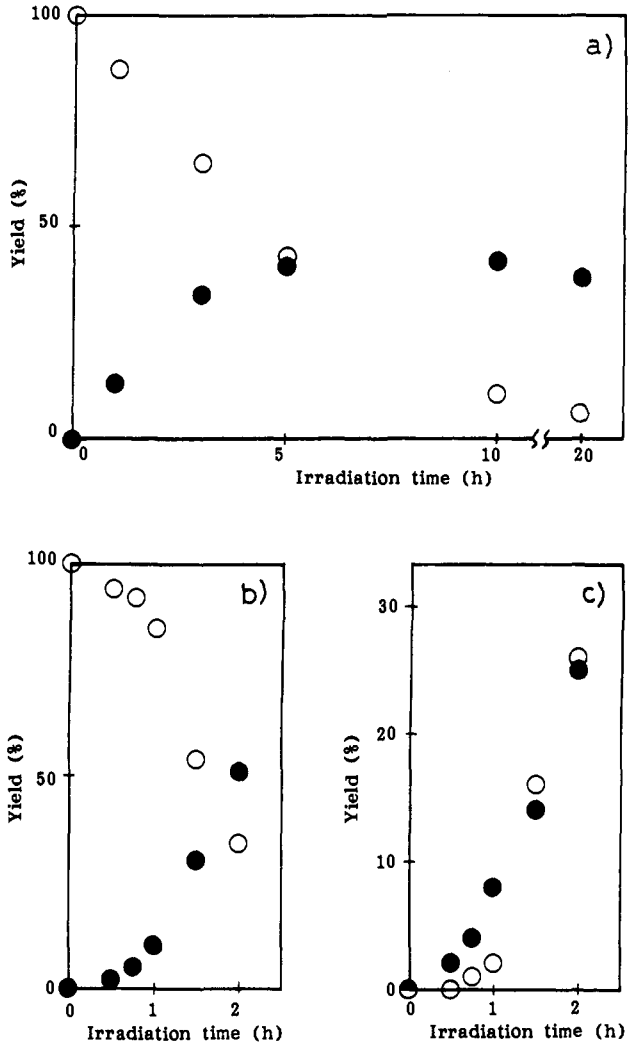

Figure 2. (a) Time course of the solid-state reaction of the *m*DV·**1** crystal. The yields of **2m** (filled circle) and recovery of *m*DV (open circle) are plotted as a function of irradiation time ($\lambda > 540$ nm). (b) Time course of the solid-state reaction of the *p*DV·**1** crystal. The combined yields of products (**2p** and **6**) (filled circle) and recovery of *p*DV (open circle) are plotted as a function of irradiation time ($\lambda > 540$ nm). (c) Irradiation time dependence of the product distribution (**2p**, filled circle; **6**, open circle) during the photolysis of the *p*DV·**1** crystal. The yields of **6** in b and c are based on *p*DV, so that its chemical yields are twice those shown in the figures. Please note that as much as 77% of **1** was consumed on irradiation of *p*DV·**1** for 2 h.

irradiation of the CT crystal. As shown above for *o*DV·**1** and ST·**1**, characteristic features in the solid-state photochemistry are the higher reaction efficiency than in solution and the regiospecific formation of a sole product under the topochemical control by the crystal lattice. However, these features are not always true as exemplified by the photoreactions of *m*DV·**1** and *p*DV·**1**. In contrast to the case of *o*DV·**1**, the *m*DV·**1** crystal afforded only 15% of **2m** on irradiation for 1 h ($\lambda > 540$ nm), showing that the reaction is rather sluggish in *m*DV·**1**. The yield of **2m** reached the maximum value (ca. 45%) after 5 h of irradiation, although *m*DV was consumed gradually upon prolonged irradiation (Figure 2a). More outstanding is the behavior of the *p*DV·**1** crystal, which was much more inert to photoirradiation at the initial stage (Figure 2b). Prolonged irradiation ($\lambda > 540$ nm, 2 h) caused the formation of not only the usual adduct **2p** (25%) but also a considerable amount of the 1:2 adduct **6** (26% based on *p*DV). The latter product was never formed on excitation of the corresponding EDA complex in MeCN. Furthermore, this solid-state reaction of *p*DV·**1** was proven to be defects-accelerated as shown by the presence of the induction

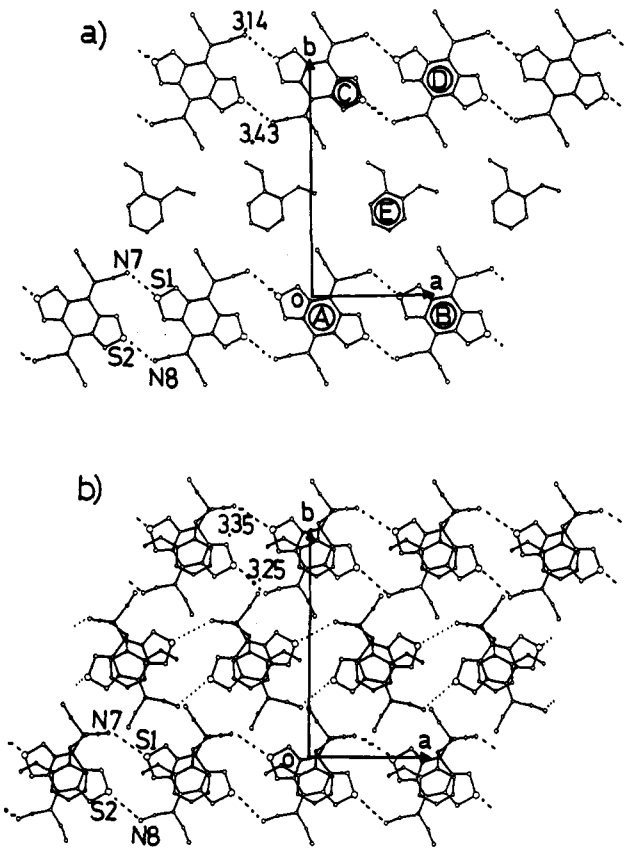

Figure 3. (a) Molecular arrangement in the *o*DV·**1** crystal viewed along the *c* axis. Linear "ribbon" networks of **1** are formed by S--N≡C contacts. The distances for S--N and the angles for the S–N–C atomic array are 3.14 Å and 114.8° for S(1)--N(7)≡C(11) and 3.43 Å and 106.2° for S(2)--N(8)≡C(12), respectively. The interplanar distances and dihedral angles between neighboring molecular planes are as follows: 1.64 Å and 0° for A and B; 3.15 Å and 22.0° for A and E; 1.51 Å and 22.0° for B and E; 0.41 Å and 22.0° for C and E; 2.05 Å and 22.0° for D and E. (b) Molecular arrangement in the chiral-**2o** crystal viewed along the *c* axis. The distances for S--N and the angles for the S–N–C atomic array are 3.35 Å and 117.6° for S(1)--N(7)≡C(11) and 3.25 Å and 117.0° for S(2)--N(8)≡C(12), respectively.

period for the reaction,[22] and the irradiation-time dependence of the product yields suggests that the 1:2 adduct **6** is the secondary product from the 1:1 adduct **2p** (Figure 2c).

These differences in the solid-state reactions of DV·**1** crystals are in sharp contrast to the similarity in the photoreactions of EDA complexes in solution and may be accounted for by the control of the reaction sequence by the crystal lattice. In the following sections, the X-ray structural determinations of the three isomeric DV·**1** crystals were carried out in order to clarify the structure–reactivity relationship as well as unique characteristics of the solid-state reactions.

Asymmetric Molecular Arrangement in the *o*DV·1 CT Crystal. In the crystal of *o*DV·**1**, linear "ribbon" networks are formed by S--N≡C contacts of **1** (3.14 and 3.43 Å)[23] along the *a* axis (Figure 3a). Molecules of *o*DV are incorporated in the cavity formed between the two "ribbons". This type of molecular arrangement is quite common in the CT crystals of **1** with aromatic hydrocarbons.[16] The noteworthy structural feature in this case is the asymmetric nature of the inclusion lattice because of the adoption of a chiral space group ($P2_1$). In other words, the achiral donor (*o*DV) is included in the chiral cave formed by the achiral

(22) Another explanation for the photoreactivity of *p*DV·**1** might be that the phase transformation would be induced upon prolonged irradiation.

(23) Sum of van der Waals radii for S--N is 3.35 Å. Pauling, L. In *The Nature of Chemical Bond*, 3rd ed.; Cornell University Press: Ithaca, NY, 1960; pp 260.

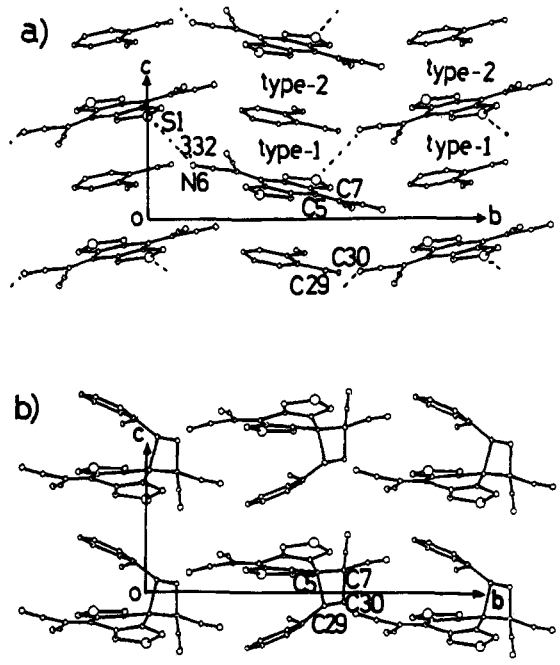

Figure 4. (a) One-dimensional columnar stack in the *o*DV·**1** crystal (*a* projection). Two kinds of overlaps (type 1 and type 2) are aligned alternately along the *c* axis. Their mirror images (type $\bar{1}$ and type $\bar{2}$) do not coexist in the same crystal due to the adoption of a chiral space group. Interatomic contacts of S(1)--N(6)≡C(10) (3.32 Å) are shown by broken lines. (b) Molecular arrangement in chiral-**2o** viewed along the *a* axis. Please note that the cycloaddition proceeds via the type 2 overlap in *o*DV·**1**.

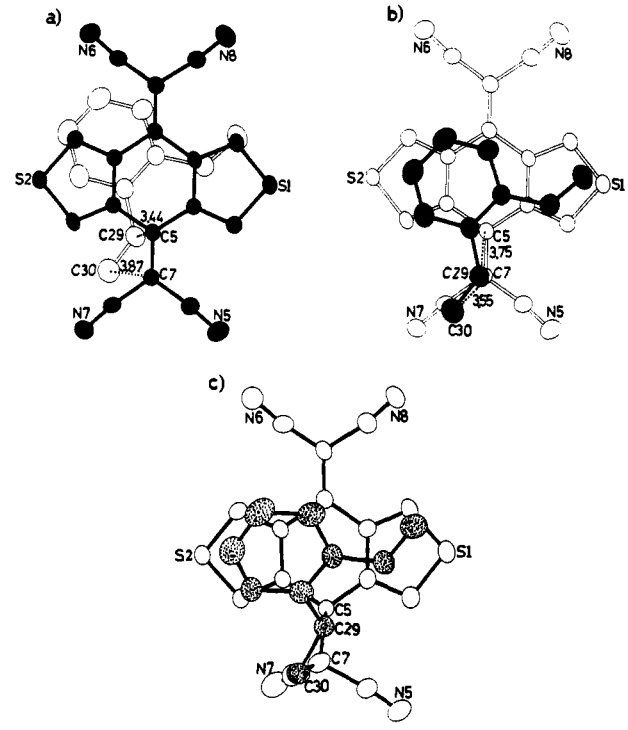

Figure 5. Two kinds of molecular overlaps in *o*DV·**1** [type 1 in a and type 2 in b]. The interplanar distances and dihedral angles are 3.40 Å and 2.6° in type 1 and 3.44 Å and 2.6° in type 2. Molecular structure of chiral-**2o** is shown in c, and the bond lengths of C(5)–C(29) and C(7)–C(30) are 1.66(2) and 1.55(2) Å, respectively.

acceptor molecule (**1**) in this crystal. Perpendicular to this arrangement are formed one-dimensional mixed stacks along the *c* axis, and two types of molecular overlaps (type 1 and type 2) are repeated alternately in the stack (Figure 4a). Two olefinic parts are aligned nearly in parallel in both overlaps with the interatomic distances of 3.44–3.87 Å (Figure 5a,b). These features of molecular arrangements meet the requirements for the [2 + 2] cycloaddition reactions of olefins in the solid state (Schmidt's rule).[24] Further analyses were made on these overlaps by elaborating the geometries of the relevant p-orbitals.[25] The distances between the apices of the p-lobes are 1.00 and 1.93 Å in type 1 and 1.32 and 1.08 Å in type 2, respectively, for C(5)--C(29) and C(7)--C(30) contacts. These values indicate the spatial proximity of orbitals in both molecular overlaps, which may result in the high reaction efficiency in the crystal. On the other hand, the regiochemistry of **2o** can be accounted for by these molecular arrangements even if the cycloaddition proceeds via the overlap of type 1 or type 2, or via both. However, the high isolated yield of **2o** (91%) could not be rationalized when both overlaps are conducive to photoreactivity in the same magnitude.[26] In such a case, a considerable amount of **1** and *o*DV would be removed from the reaction and left unreacted between the adducts in the stack (Scheme 2a→b). Thus, the cycloaddition was suggested to proceed predominantly via one of the two overlaps, and it is of further interest to determine which overlap favors the cycloaddition. The closest contact [C(5)--C(29) 3.44 Å] between the reactive sites is found in type 1, whereas type 2 seems more favorable for ET from the HOMO of *o*DV to the LUMO of **1** by considering the MO coefficients.[16] In order to investigate the detailed reaction pathway in the crystal, the photoreaction was followed by the X-ray diffraction technique.

Scheme 2

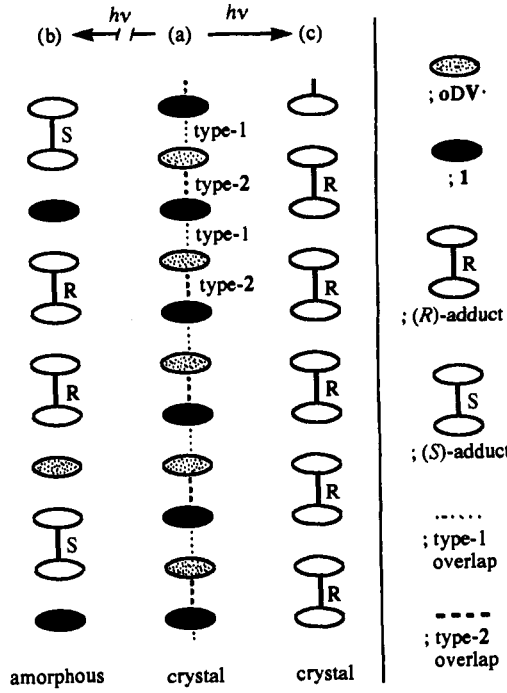

Single Crystal-to-Single Crystal Transformation of *o*DV·1 into Adduct 2o. The powder X-ray analyses revealed that the high crystallinity was maintained during the course of the cycloaddition in *o*DV·**1** (Figure 6). This result is in accord with the assumption that one of the two overlaps is much more favorable for the cycloaddition than the other (Scheme 2a→c). It is also noteworthy that the "as-prepared" adduct **2o** (Figure 6c, conversion 84%)

(24) Schmidt, G. M. J. *Pure Appl. Chem.* **1971**, *27*, 647.
(25) Kearsley, S. K. In *Organic Solid State Reactions: The Prediction of Chemical Reactivity within Organic Crystals using Geometrical Criteria*; Desiraju, G. R., Ed.; Elsevier: Amsterdam, 1987; pp 69–115. The positions of the p-orbital apices were constructed by using the olefinic plane normal with a distance of 1.8 Å from the carbon atom. Sum of the distances for a set of double bonds would be less than 3.5 Å in reactive crystals.
(26) The theoretical maximum yield was reported to be 86.5% for the solid-state [2 + 2] photodimerization reaction in the idealized stack-type crystal structure, Wernick, D. L.; Schochet, S. *J. Phys. Chem.* **1988**, *92*, 6773.

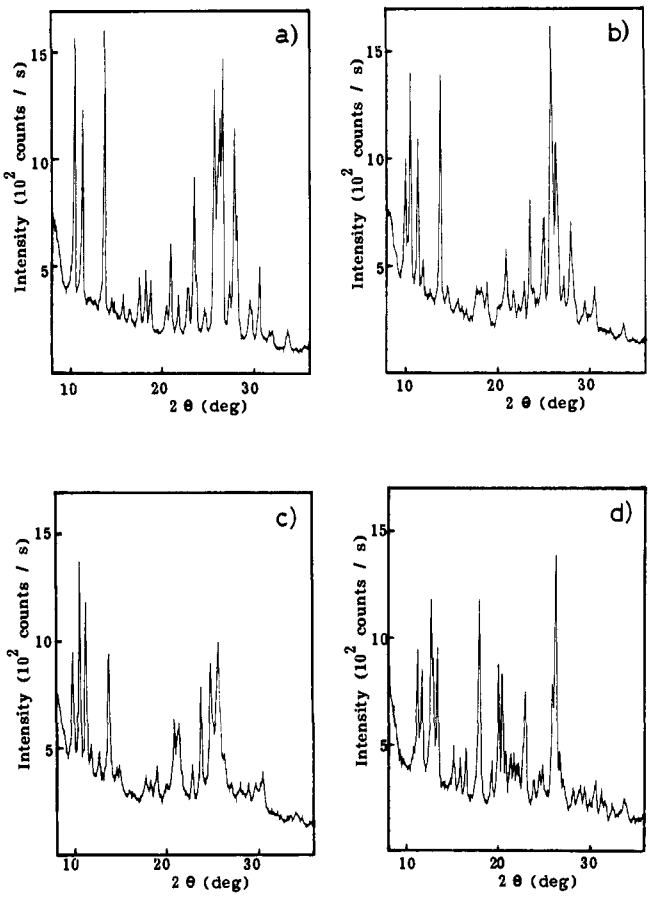

Figure 6. Continuous changes in X-ray powder diffraction patterns (Cu Kα) of the *o*DV·**1** crystal on irradiation (λ > 540 nm): (a) before irradiation; (b) after 5 min, conversion 48%; (c) after 15 min, conversion 84%. The diffraction pattern in d is that of adduct **2o** after recrystallization. Please note the difference between the as-prepared adduct (chiral-**2o**) in c and *dl*-**2o** in d.

exhibited a diffraction pattern quite dissimilar to that of the recrystallized adduct (Figure 6d).[27] The latter was found to be the *dl*-crystal of **2o** (*dl*-**2o**) involved in the centrosymmetric crystal structure of the $P2_1/n$ space group (Table 2). These results indicate that the crystal chirality in *o*DV·**1** was maintained in the as-prepared adduct **2o** by the crystal-to-crystal transformation, but the dissolution–crystallization process caused the loss of crystal chirality in giving *dl*-**2o** (racemic compound) because the powder sample of the as-prepared adduct was a racemic mixture of the right- and left-handed crystals.

On irradiations of the single crystals of *o*DV·**1**, the color of the crystals gradually changed from deep red to pale yellow with the proceeding of the photoreaction. It is of interest that all the samples kept a clear appearance and never became opaque although several specimens suffered cracking of the crystals into tiny pieces. The latter finding suggests that the cycloaddition in *o*DV·**1** proceeds via the single crystal-to-single crystal transformation, and fortunately, we have succeeded in obtaining a crystal of the as-prepared adduct which has a size enough for X-ray crystallography.

Comparisons of crystal data indicate that the as-prepared adduct **2o** is isomorphous to that of *o*DV·**1**, suggesting that the cycloaddition is akin to the topotactic transformation (Table 2). Figure 3b shows the molecular arrangement viewed along the *c* axis in the as-prepared adduct **2o** (chiral-**2o**). As in the case of *o*DV·**1**, molecules of **2o** are connected along the *a* axis by S--N≡C contacts (3.25 and 3.35 Å). The striking resemblance of

(27) It was observed that the crystal structure of the "as-prepared" product is different from that of the recrystallized form (solvated crystal) of 2-benzyl-5-benzylidenecyclopentanone photodimer (ref 14).

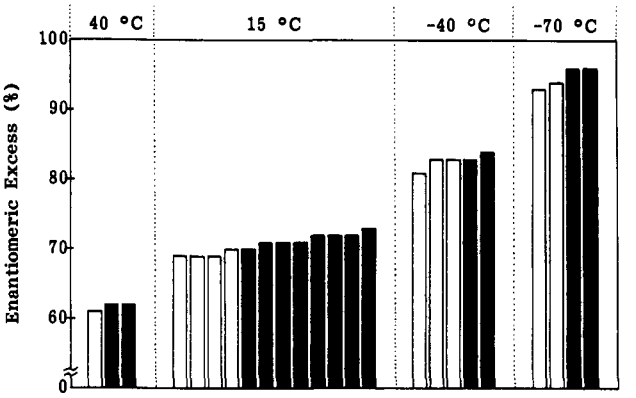

Figure 7. Bargraph representation of the enantiomeric excess (ee) for adduct **2o** obtained by the absolute asymmetric synthesis at four different temperatures. Each open or filled bar denotes the ee value of one specimen having the optical rotatory power of (+) or (–), respectively.

molecular arrangements shows that the cycloaddition occurred without a significant change of the crystal matrix formed by **1** in the *o*DV·**1** crystal. Only slight movement of reactive sites along the stacking *c* axis enables the cycloaddition of *o*DV and **1**, which allows the topochemical and single crystal-to-single crystal transformation of *o*DV·**1** to the chiral-**2o** crystal. These results indicate the stereospecific nature of the cycloaddition because the rotation or inversion of the molecular halves in a plausible reaction intermediate is impossible within the network formed by S--N≡C contacts. Comparisons of molecular arrangements afforded the direct evidence that the cycloaddition proceeds predominantly via the type 2 overlap in *o*DV·**1** (Figure 4b and 5c). This fact suggests that the stronger CT interaction through the face-to-face overlap plays a more important role than the closest atomic contact between the reactive sites in the case of the cycloaddition induced by ET.

Absolute Asymmetric Synthesis of Adduct 2o. The topochemical and stereospecific cycloaddition allows the transfer of crystal chirality in *o*DV·**1** to adduct **2o** as the molecular chirality by the covalent bonding (an asymmetric center on the aryl-substituted methine carbon). That is, a certain single crystal of *o*DV·**1** possessing the molecular overlaps of types 1 and 2 will afford (*R*)-**2o** as a major stereoisomer because of the selective addition via type 2 as well as the absence of the mirror images of molecular overlaps (types $\bar{1}$ and $\bar{2}$) in the same crystal. Adduct **2o** with (*S*)-configuration will be obtained from another single crystal possessing the types $\bar{1}$ and $\bar{2}$ overlaps by the selective cycloaddition via type $\bar{2}$. Usually adduct **2o** obtained by photoirradiation on the powder sample of *o*DV·**1** had no optical rotatory power because complexation of **1** with *o*DV afforded a racemic mixture of right- and left-handed CT crystals without self-inoculation. However, the absolute asymmetric synthesis of **2o** could be realized on irradiation of a grown single crystal of *o*DV·**1**.

When 12 specimens of *o*DV·**1** single crystals were irradiated piece by piece at 15 °C (λ > 540 nm), the resulting adduct **2o** exhibited high optical purity (av 71% ee, $[\alpha]_D^{20} = 117°$)[28] with both signs of optical rotation (Figure 7). Because the values of enantiomeric excess were quite reproducible and clustered in the narrow range of 69–73%, the defects or twinning of the single crystals are not responsible to the observed lowering of optical purities. Furthermore, the racemization of **2o** was not indicated under the ambient conditions or by its purification on SiO_2. Thus, the optical yield of 71% is intrinsic for the solid-state cycloaddition of *o*DV·**1** at 15 °C, corresponding to the relative reactivities for the two overlaps, type 1:type 2 = 15:85.

(28) Eight specimens having the same chirality (longer retention time in HPLC) were combined followed by the reexamination of ee (71%) by HPLC. For this sample was obtained the α value of –0.117° in $CHCl_3$ (c = 0.1) at 20 °C. The authors are grateful to Prof. Kuninobu Kabuto, Tohoku University, for his help in the polarimetric measurements.

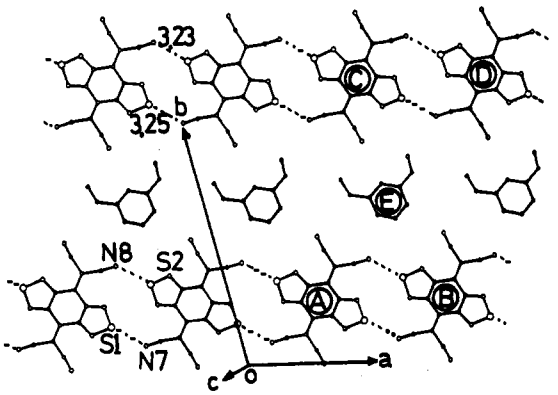

Figure 8. Molecular arrangement in the *m*DV·**1** crystal showing the "ribbon" networks formed by S--N≡C contacts. The distances for S--N and the angles for the S–N–C atomic array are 3.25 Å and 122.2° for S(1)--N(7)≡C(11) and 3.23 Å and 122.0° for S(2)--N(8)≡C(12), respectively. The interplanar distances and dihedral angles between neighboring molecular planes are as follows: 1.40 Å and 0° for A and B; 0.36 Å and 1.4° for A and E; 1.03 Å and 1.4° for B and E; 0.49 Å and 1.4° for C and E; 0.90 Å and 1.4° for D and E.

Temperature dependence of the enantiomeric excess (ee) was examined in order to investigate the effect of thermal motion in the crystal[29] on the relative reactivities for the two overlaps. Again the reproducible values of ee were obtained at the same temperature with both signs of optical rotation, and the averaged values are 62%, 71%, 83%, and 95%, respectively, at 40 °C, 15 °C, –40 °C, and –70 °C. These values clearly show that the optical yields keep rising steadily with lowering of the reaction temperature. The relative reactivities (type 2:type 1) at these temperatures were deduced as 4.3, 5.9, 11, and 39, respectively, which are indicative of the suppression of the type 1 reactivity by a decrease in thermal motion in the crystal. This phenomenon is probably related with the fact that larger shifts of atomic positions are required to connect C(30) of *o*DV and C(7) of **1** (3.87 Å) in the type 1 overlap. Furthermore, lowering the temperature increases the CT interaction between *o*DV and **1**,[30] which seems advantageous to the cycloaddition via the type 2 overlap because of the matching of the MO coefficients. Both factors are favorable for the cycloaddition via type 2 at lower temperatures, which can account for the observed temperature dependence of ee.

When a single crystal of *o*DV·**1** as a seed was added to the oversaturated solutions of **1** in neat *o*DV, optically enriched CT crystals could be obtained, which afforded (+)- and (–)-**2o** in bulk after irradiation at 15 °C. However, the optical purities were as low as ca. 10% ee, showing that the inoculation was not sufficient to realize the complete entrainment on complexation. Finally, the absolute configuration of the selected single crystal of *o*DV·**1** for crystallography was successfully determined as shown in the figures by using the anomalous scattering of *S* with Cu Kα radiation ($\Delta f'' = 0.557$).[31] Because the same specimen afforded (+)-**2o** on irradiation, the absolute configuration of **2o** could be deduced as (*R*)-(+)-**2o** by considering the predominant cycloaddition via the type 2 overlap in *o*DV·**1**.

Crystal Structure and Crystal-to-Amorphous Transformation of the *m*DV·1 CT Crystal. The X-ray analysis of the *m*DV·**1** CT crystal revealed the formation of infinite "ribbon" networks of **1** by S--N≡C contacts (3.25 and 3.23 Å)[23] along the *a* axis, and *m*DV molecules are incorporated between the two ribbons on the (01$\bar{1}$) plane (Figure 8). Along the *c* axis are formed one-dimensional mixed columns, in which **1** and *m*DV are stacked alternately, resulting in the two different types of face-to-face

(29) For the temperature dependence of the solid-state [2 + 2] photoreactions, see: Dhurjati, M. S. K.; Sarma, J. A. R. P.; Desiraju, G. R. *J. Chem. Soc., Chem. Commun.* **1991**, 1702. Chung, C.-M.; Nakamura, F.; Hashimoto, Y.; Hasegawa, M. *Chem. Lett.* **1991**, 779.

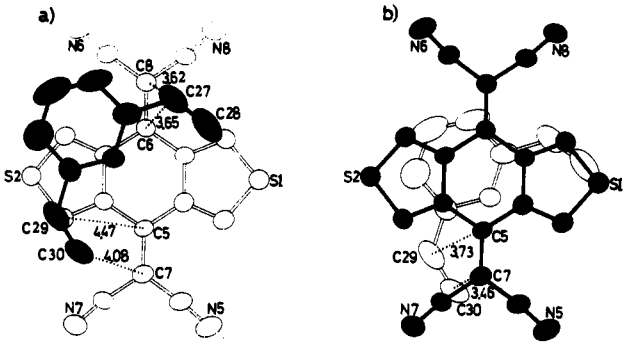

Figure 9. Two kinds of molecular overlaps in *m*DV·**1** [type 1 in a and type 2 in b]. The interplanar distances and dihedral angles are 3.46 Å and 1.4° in type 1 and 3.38 Å and 1.4° in type 2.

overlappings (Figure 9). These structural features are quite similar to those in the *o*DV·**1** crystal, but the absolute asymmetric synthesis cannot be expected in this case because of the adoption of a centrosymmetric packing arrangement (space group $P\bar{1}$). That is, if the cycloaddition occurs selectively via one of these two overlaps (type 1 or type 2), there exists the same number of their mirror images (type $\bar{1}$ and type $\bar{2}$) in the same crystal, which results in the formation of the racemic compound.

Both of two overlaps are favorable for the interaction between HOMO (*m*DV) and LUMO (**1**) by considering the MO coefficients. However, the overlap integral seems larger in type 2 because of the shorter interplanar distance (3.46 Å in type 1 and 3.38 Å in type 2) as well as the slipping of molecular planes in type 1. Moreover, the distances between the reactive sites are much shorter in type 2 [C(7)--C(30), 3.46 Å; C(5)--C(29), 3.73 Å] than in type 1 [C(7)--C(30), 4.08 Å; C(5)--C(29), 4.47 Å; C(6)--C(27), 3.65 Å; C(8)--C(27), 3.62 Å],[32] suggesting that the cycloaddition may occur predominantly via type 2. The regioselective formation of **2m** on irradiation is in accord with the fact that the type 2 overlap is favorable for the formation of **2m** but not its regioisomer **3m**.

The distinct structural feature in *m*DV·**1** is the considerable coplanarity of the molecular arrangement on the (01$\bar{1}$) plane shown in Figure 8. The molecules on this plane are aligned almost in parallel (dihedral angles < 1.4°), and the largest deviation between the neighboring molecular planes is only 1.40 Å. These values are much smaller than the corresponding values for the similar arrangement in *o*DV·**1** (22° and 3.15 Å in Figure 3a). Although the addition of *m*DV and **1** occurs perpendicularly to this plane, translation and slight rotation of the aryl moiety of *m*DV are needed on this plane to connect C(5) and C(29) in the type 2 overlap, so that such a compact arrangement seems unfavorable for the cycloaddition, thus lowering the apparent reactivity of *m*DV·**1** compared with *o*DV·**1**. Once adduct **2m** is formed, it seems likely that the molecular arrangement would suffer a considerable change in order to accommodate the product. Thus, the crystallinity is gradually diminished with the progress of cycloaddition, which was indicated by the changes of X-ray powder diffraction patterns (Figure 10). These environmental changes with the crystal-to-amorphous transformation may be related with the low maximum yield of **2m** on irradiation.

Crystal Structure and Photoreactivity of the *p*DV·1 CT Crystal. In the crystal of *p*DV·**1**, each of components lies on a crystallographic center of symmetry. Vinyl moieties of *p*DV are positionally disordered. As shown in Figure 11, the coplanar

(30) A one and a half times increase in K_{CT} was observed by lowering the temperature from 30 to 0 °C for the EDA complex of **1** with *p*-xylene (ref 16).

(31) *International Tables for X-ray Crystallography;* Kynoch Press: Birmingham, 1974; Vol. IV, pp 149.

(32) The distances between the apices of the p-orbitals are 2.87 and 2.29 Å in type 1, and 1.63 and 0.72 Å in type 2, respectively, for C(5)--C(29) and C(7)--C(30) contacts, which also indicate that the type 2 overlap is more conducive to cycloaddition.

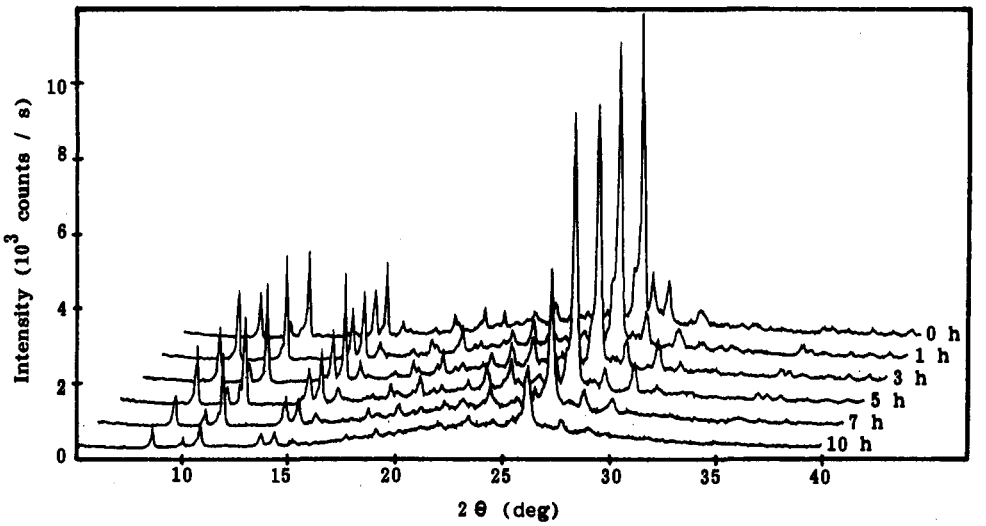

Figure 10. Time course of the X-ray powder diffraction pattern (Cu Kα) on irradiation of the *m*DV·**1** crystal (λ > 540 nm). The isolated yields of the adduct **2m** at each reaction period are as follows: 1 h, 6%; 3 h, 16%; 5 h, 20%; 7 h, 28%; 10 h, 30%. Please note the diminution of crystallinity in the samples irradiated for 7 and 10 h.

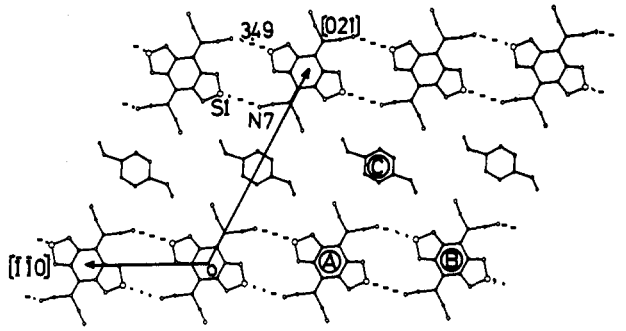

Figure 11. Molecular arrangement in the *p*DV·**1** crystal showing the loose "ribbon" networks of **1**. The distance for S(1)--N(7) is 3.49 Å, which is much longer than the sum of van der Waals radii. The angle for the S(1)–N(7)–C(11) atomic array is 149.6°. Disordered vinyl groups in *p*DV are shown by one of three possible positions [C(21)—C(241)═C-(251)]. The interplanar distances and dihedral angles between neighboring molecular planes are as follows: 0.67 Å and 0° for A and B; 0.01 Å and 2.3° for A and C; 0.68 Å and 2.3° for B and C.

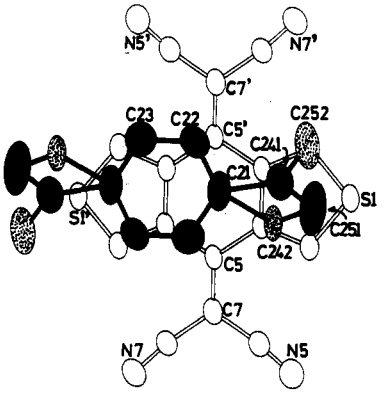

Figure 12. Molecular overlap in *p*DV·**1** showing the disordered atomic positions for the vinyl groups. Three different positions adopted are as follows: C(21)—C(241)═C(251), C(21)—C(241)═C(252), and C(21)—C(242)═C(251). The interplanar distance between two molecular planes is 3.37 Å with the dihedral angle of 2.5°. This overlap is not suitable for the interaction between the HOMO (*p*DV) and LUMO (**1**). The interatomic distances between the two olefinic parts are as follows: C(5')--C(241), 3.96 Å; C(7')--C(252), 4.40 Å; C(7')--C(251), 5.25 Å; C(5)--C(242), 3.77 Å; C(7)--C(251), 4.97 Å. The distances between the apices of the p-orbitals are 1.94, 2.62, 3.79, 1.80, and 3.47 Å, respectively, for the above five contacts.

arrangement of molecules is observed on the (1$\bar{1}$2) plane, and the one-dimensional mixed column is formed along the *c* axis. These structural features indicate that the molecular packing of isomeric DV·**1** crystals is essentially the same and characterized by the "ribbon" network of **1** as well as the mixed columnar stack with face-to-face overlapping.

In accord with the photoinertness at the initial stage (Figure 2b), the molecular overlap in *p*DV·**1** seems quite unfavorable for the cycloaddition. As shown in Figure 12, the long axis of *p*DV is directed parallel to the short axis of the TCNQ (tetracyanoquinodimethane) skeleton of **1**, thus the olefinic parts of *p*DV and **1** are arranged almost perpendicularly, resulting in rather long distances between them to be connected (3.77–5.25 Å). However, the interatomic distance for S--N≡C (3.49 Å) in this crystal is much longer than the sum of van der Waals radii (3.35 Å)[23] or those in other CT crystals of **1**,[33] showing that the "ribbon" network in *p*DV·**1** is quite looser than those in *o*DV·**1** and *m*DV·**1**. Furthermore, the disorder of the vinyl groups indicates the presence of the unoccupied large space in the cave, which is also suggested by the lowest density of *p*DV·**1** among three isomeric DV·**1** CT crystals (Table 2). Such a loose inclusion cavity may allow the in-plane rotation of the benzene nucleus of *p*DV, that accounts for the formation of **2p** in spite of the unfavorable overlapping pattern. It is also noteworthy that the induction period for the cycloaddition in the *p*DV·**1** crystal varied from sample to sample. On irradiation with λ > 540 nm for 2 h, the sample obtained by the rapid direct method afforded **2p** and **6** in total 51% yield based on *p*DV (77% based on **1**, Figure 2a). However, the combined yield of the products was only one-third when the well-ground sample of slowly grown single crystals was irradiated for 2 h under the same conditions (16% based on *p*DV; 25% based on **1**). Such a sample dependence suggests that the addition occurs at the lattice defects even in the early stage of the photoreaction. As the reaction proceeds, the increase in defects is expected in order to accommodate the products in the molecular arrangements, that will facilitate the cycloaddition of *p*DV and **1** around the defects.

The striking feature of the photoreaction in *p*DV·**1** is the formation of the 1:2 adduct **6** in pretty good yield, which can be accounted for by the electrochemical properties of the 1:1 adduct **2p**. Comparisons of the cyclic voltammograms indicate that **2p** undergoes one-electron oxidation more easily than its geometrical

(33) The distances for S--N≡C contacts are as follows: 3.04 Å in neutral **1**, 3.28 and 3.40 Å in the benzene·**1** complex, 3.22 and 3.24 Å in the *p*-xylene·**1** complex, 3.19 and 3.35 Å in the *o*-methylanisole·**1** complex, 3.25 Å in the *p*-methylanisole·**1** complex, 3.28 Å in the 2,6-dimethylnaphthalene·**1** complex, 3.19 and 3.21 Å in the 2,7-dimethylnaphthalene·**1** complex (ref 16).

isomer **2o** or **2m**,[34] and its oxidation potential (+1.86 V) is lower than that of ST and close to those of *o*DV and *m*DV. This fact indicates that ET from **2p** to **1** might occur under the irradiation conditions ($\lambda > 540$ nm), leading to the further cycloaddition of **2p** with **1** to form **6**.[35] The absence of **6** on the photolysis in MeCN can be accounted for by the negligible formation of the EDA complex between **2p** and **1** because of the low concentration of the adduct **2p** even after 5-h irradiation (ca. 8×10^{-4} mol dm^{-3}). On the other hand, the styryl moiety of **2p** formed in the crystal is just facing another molecule of **1** because the one-dimensional mixed stack is initially formed in *p*DV·**1**. Such an intimate arrangement is advantageous in forming **6** in the crystal form.

Conclusion

This work revealed the intriguing facets of CT crystals which serve as novel photoreactive substances. Because their photoreactions proceed upon excitation of the CT bands, it is most probable that the ET process is responsible for initiating the observed chemical reactions in the solid state. The intimate arrangement of donor and acceptor molecules in the crystal is quite suitable for ET, and the apparent reactivity is much higher than that in solution in the favorable cases such as the cycloaddition reactions in *o*DV·**1** and ST·**1** crystals.

The photoreactions examined here also exhibited several characteristic features of the solid-state reactions such as the asymmetric synthesis of the adduct **2o** in *o*DV·**1**, and the 1:2 adduct **6** obtained on irradiation of *p*DV·**1** is hardly accessible during the photoreactions in solution. In spite of the similarity in solution photochemistry of EDA complexes, the topochemical control of the reaction sequences also caused the variety in the solid-state reactivities of DV isomers included in the spatial cavities formed by S--N≡C contacts of **1**. The S--N≡C interaction may also take part in maintaining the crystal matrix during the photoconversion of *o*DV·**1** to chiral-**2o**, thus endowing the CT crystals with additional properties.

Although the [2 + 2]-type cycloaddition is the sole reaction mode observed in this work, a variety of other reactions can be expected from radical ion pairs formed on irradiation of CT crystals. Studies in this vein are now in progress to explore this undeveloped category of photochemistry.

Experimental Section

General. ^{1}H NMR and ^{13}C NMR spectra were recorded at 200 and 50 MHz, respectively. MS spectra were obtained in the EI mode at 70 eV unless indicated otherwise. These spectral measurements as well as elemental analyses were carried out at the Instrumental Analysis Center for Chemistry, Faculty of Science, Tohoku University. Melting points are reported uncorrected. All the IR spectra were taken using KBr disks. Preparative thick-layer chromatography (TLC) was performed on 0.5 mm × 20 cm × 20 cm SiO_2 plates. All the photoirradiations were conducted by using a 2-kW xenon lamp with an appropriate glass cutoff filter.

Materials. BTDA (**1**) was prepared by the condensation reaction of the corresponding diketone and malononitrile as reported previously[16] and purified by gradient sublimation onto Teflon. Divinylbenzenes (DVs) were prepared via Wittig reactions, as described for *p*DV.[36] *p*DV was purified by chromatographic separation on SiO_2 (*n*-hexane), and *o*DV (bp 79–80 °C, 16 mmHg) and *m*DV (bp 81.5–82 °C, 15 mmHg) were purified by distillation. ST was purchased and used as received. MeCN was dried over CaH_2 and distilled before each use for the photoreaction.

Preparation of CT Crystals of BTDA (1) with Arylolefins. Finely powdered **1** (200 mg, 0.63 mmol) was suspended in 2 mL of CH_2Cl_2 containing *p*DV (164 mg, 1.26 mmol), and the solvent was gradually evaporated until the color of the suspension turned brownish purple. After the mixture was allowed to stand for 12 h, the dark purple powder of *p*DV·**1** (283 mg, 100%) was obtained by removal of the solvent and excess *p*DV in vacuo for 3 h at room temperature. Single crystals of *p*DV·**1** were also obtained as purple plates by recrystallizing **1** from MeCN containing excess *p*DV in 76% yield.

Other CT crystals [*m*DV·**1** (phase A), *o*DV·**1**, and ST·**1**] were prepared in quantitative yields by admixing **1** with neat arylolefins followed by evaporation of excess volatile donors in vacuo. Single crystals of mDV$_5$·**1**$_3$ (phase B) were obtained as orange plates by the vapor diffusion method in MeCN/*n*-hexane accompanied with red needles of *m*DV·**1** (phase A).

*p*DV·**1**: mp 168–174 °C dec; IR 2215 cm^{-1}. Anal. Calcd for $C_{22}H_{10}N_8S_2$ (1:1): C, 58.66; H, 2.24; N, 24.87. Found: C, 58.42; H, 2.35; N, 24.75.

*m*DV·**1** (phase A): red powder, mp 95–98 °C dec; IR 2215 cm^{-1}. Anal. Calcd for $C_{22}H_{10}N_8S_2$ (1:1): C, 58.66; H, 2.24; N, 24.87. Found: C, 58.90; H, 2.49; N, 24.54.

*o*DV·**1**: red powder, mp 95–98 °C dec; IR 2220 cm^{-1}. Anal. Calcd for $C_{22}H_{10}N_8S_2$ (1:1): C, 58.66; H, 2.24; N, 24.87. Found: C, 58.45; H, 2.36; N, 24.72.

ST·1: orange powder, mp 82–86 °C dec; IR 2220 cm^{-1}. Anal. Calcd for $C_{20}H_8N_8S_2$ (1:1): C, 56.59; H, 1.90; N, 26.40. Found: C, 56.04; H, 2.15; N, 26.00.

mDV$_5$·**1**$_3$ (phase B): mp 96–102 °C dec; IR 2215 cm^{-1}. Anal. Calcd for $C_{86}H_{50}N_{24}S_6$ (5:3): C, 64.08; H, 3.13; N, 20.86. Found: C, 63.36; H, 3.37; N, 20.94.

CT Excitation Reactions of EDA Complexes in MeCN. A solution of *p*DV (65 mg, 0.5 mmol) and **1** (32 mg, 0.1 mmol) in MeCN (10 mL) was irradiated ($\lambda > 450$ nm) for 5 h at 20 °C under nitrogen. After the photolysis, the reaction mixture was concentrated in vacuo. The recovery of *p*DV (82%) was determined on the basis of the ^{1}H NMR spectrum by using 1,1,1,2-tetrachloroethane as an internal standard. The photolysate was digested with CH_2Cl_2 (2 mL), and unreacted **1** (21 mg, 67%) was recovered as a yellow powder by filtration. From the filtrate was obtained **2p** (3.6 mg) by preparative TLC (CH_2Cl_2) in 8% yield. After a similar photolysis for 20 h, **2p** (20 mg) was isolated by preparative TLC in 44% yield. In this case, the recovery of *p*DV was only 25% (^{1}H NMR), and **1** could not be recovered from the photolysate containing traces of many undefinable products.

Photoreactions of other EDA complexes were similarly carried out in MeCN for 5 h at 20 °C ($\lambda > 450$ nm). The results summarized in Table 1 were reproducible for another run of similar experiments, and the 1:1 adducts **2** were the sole isolable products from the reaction mixtures obtained by 5 h of irradiation in all cases.

2p: yellow powder, mp 124–130 °C dec; IR 2215 cm^{-1}; ^{1}H NMR ($CDCl_3$) δ 7.17 (2 H, AA′XX′), 6.71 (2 H, AA′XX′), 6.55 (1 H, dd, J = 11.0, 17.6 Hz), 5.64 (1 H, dd, J = 0.6, 17.6 Hz), 5.38 (1 H, dd, J = 9.0, 12.0 Hz), 5.22 (1 H, dd, J = 0.6, 11.0 Hz), 4.29 (1 H, dd, J = 12.0, 12.0 Hz), 3.36 (1 H, dd, J = 9.0, 12.0 Hz); ^{13}C NMR ($CDCl_3$) δ 157.55, 155.87, 150.94, 150.10, 138.18, 137.78, 135.53, 133.11, 126.73, 126.51, 115.13, 112.89, 112.51, 112.46, 112.12, 84.56, 56.15, 49.24, 36.70, 33.92; UV (MeCN) λ_{max} = 350 (ϵ 14 000), 324 (17 100), 280 sh (19 200), 258 (26 600), 236 sh (19 100) nm; MS m/z (relative intensity) 372 ($M^+ - CH_2{=}C(CN)_2$, 69), 371 ($M^+ - CH_2{=}C(CN)_2 - 1$, 100), 346 ($M^+ - CH_2{=}C(CN)_2 - CN$, 15), 345 ($M^+ - CH_2{=}C(CN)_2 - CN - 1$, 23). Anal. Calcd for $C_{22}H_{10}N_8S_2$: C, 58.66; H, 2.24; N, 24.87. Found: C, 58.74; H, 2.63; N, 24.44.

2m: yellow powder, mp 157–162 °C dec; IR 2215 cm^{-1}; ^{1}H NMR ($CDCl_3$) δ 7.22 (1 H, d, J = 7.8 Hz), 7.08 (1 H, dd, J = 7.6, 7.8 Hz), 6.83 (1 H, s), 6.57 (1 H, d, J = 7.6 Hz), 6.54 (1 H, dd, J = 11.1, 17.6 Hz), 5.62 (1 H, dd, J = 0.5, 17.6 Hz), 5.38 (1 H, dd, J = 8.8, 12.4 Hz), 5.25 (1 H, dd, J = 0.5, 11.1 Hz), 4.34 (1 H, dd, J = 11.5, 12.4 Hz), 3.38 (1 H, dd, J = 8.8, 11.5 Hz); UV (MeCN) λ_{max} = 368 sh (ϵ 10 500), 352 (13 400), 324 (15 600), 278 (18 000), 250 (19 000), 236 sh (18 100), 214 (33 900) nm; MS m/z (relative intensity) 372 ($M^+ - CH_2{=}C(CN)_2$, 73), 371 ($M^+ - CH_2{=}C(CN)_2 - 1$, 100), 346 ($M^+ - CH_2{=}C(CN)_2 - CN$, 15), 345 ($M^+ - CH_2{=}C(CN)_2 - CN - 1$, 35). Anal. Calcd for $C_{22}H_{10}N_8S_2{\cdot}0.5H_2O$: C, 57.51; H, 2.41; N, 24.39. Found: C, 57.32; H, 2.50; N, 24.00.

(34) Redox potentials of the 1:1 adducts **2** were measured under the same conditions shown in Table 1. All the waves were irreversible, and half-wave potentials were estimated as $E^{ox} = E_p - 0.03$ and $E^{red} = E_p + 0.03$. The values of E^{ox} are >+2.2, +1.97, +1.95, and +1.86 V for **2st**, **2o**, **2m**, and **2p**, respectively, and those for E^{red} are –0.33, –0.34, –0.31, and –0.31 V. Because the oxidation potentials of **2o** and **2m** are higher than that of **2p** and rather similar to that of ST, the ET process from **2o** or **2m** to **1** in the crystal seems unfavorable under the irradiation conditions ($\lambda > 540$ nm). This idea is in consonance with the fact that the ST·**1** crystal afforded **2st** only in low yield (19%) when irradiated with light of $\lambda > 540$ nm for 1 h (71% yield with light of $\lambda > 505$ nm for 1 h).

(35) Attempts to suppress the formation of **6** by using the longer wavelength light for excitation were unsuccessful although the relative yield of **6** to **2p** was slightly reduced ($\lambda > 590$ nm, 5 h; **2p**, 29%, **6**, 22%).

(36) Nuyken, O.; Siebzehnrübl, F. *Makromol. Chem.* **1988**, *189*, 541.

2o: pale yellow powder, mp 155–158 °C dec; IR 2220 cm^{-1}; ^1H NMR ($CDCl_3$) δ 7.04–7.28 (4 H, m), 5.88 (1 H, dd, J = 10.8, 17.2 Hz), 5.34 (1 H, dd, J = 8.8, 12.0 Hz), 4.87 (1 H, dd, J = 1.2, 17.2 Hz), 4.56 (1 H, dd, J = 1.2, 10.8 Hz), 4.43 (1 H, dd, J = 12.0, 12.0 Hz), 3.41 (1 H, dd, J = 8.8, 12.0 Hz); UV (MeCN) λ_{max} = 350 (ϵ 12 800), 324 (15 600), 290 sh (14 000), 274 (16 400), 232 (18 700) nm; MS m/z (relative intensity) 450 (M^+, 6), 372 ($M^+ - CH_2{=}C(CN)_2$, 98), 345 ($M^+ - CH_2{=}C(CN)_2 - CN$, 100). Anal. Calcd for $C_{22}H_{10}N_8S_2$: C, 58.66; H, 2.24; N, 24.87. Found: C, 58.04; H, 2.47; N, 24.67.

2st: faintly yellow powder, mp 159–164 °C dec; IR 2220 cm^{-1}; ^1H NMR ($CDCl_3$) δ 7.14–7.17 (3 H, m), 6.72–6.76 (2 H, m), 5.41 (1 H, dd, J = 9.0, 12.0 Hz), 4.32 (1 H, dd, J = 12.0, 12.0 Hz), 3.38 (1 H, dd, J = 9.0, 12.0 Hz); UV (MeCN) λ_{max} = 370 sh (ϵ 10 200), 352 (13 000), 324 (15 200), 290 sh (14 800), 280 (16 100), 272 sh (15 400), 230 (10 100), 214 sh (14 700) nm; MS m/z (relative intensity) 424 (M^+, 0.4), 347 ($M^+ - CH_2{=}C(CN)_2 - 1$, 100). Anal. Calcd for $C_{20}H_8N_8S_2{\cdot}1.25H_2O$: C, 53.74; H, 2.37; N, 25.07. Found: C, 53.83; H, 2.07; N, 24.77.

CT Excitation Reactions of CT Crystals (Powder Samples). A water suspension (10 mL) of ST·**1** (42 mg, 0.1 mmol) was irradiated (λ > 505 nm) for 1 h at 15 °C. The orange powder gradually turned to yellow. Filtration of the precipitates followed by the TLC separation (CH_2Cl_2) afforded 30 mg of **2st** as a faintly yellow powder in 71% yield.

Analogously 10-mL water suspensions of *o*DV·**1** (45 mg, 0.1 mmol) were irradiated (λ > 540 nm) for 15 min and 1 h, and **2o** was isolated in 84% and 91% yield, respectively, by the TLC separation (CH_2Cl_2) of the photolysates.

In the cases of *m*DV·**1** and *p*DV·**1** CT crystals, the time courses of the photoreactions shown in Figure 2 were followed by determining the conversions in the photolysates. Thus, 5-mL water suspensions of the CT crystals (23 mg, 0.05 mmol) were irradiated separately for the period at 15 °C (λ > 540 nm), and the filtered precipitates were analyzed by ^1H NMR in acetone-d_6 (for *m*DV·**1**) and DMSO-d_6 (for *p*DV·**1**) by using 1,1,1,2-tetrachloroethane as an internal standard.

For the purpose of the isolation of the 1:2 adduct **6**, the *p*DV·**1** CT crystal (45 mg, 0.1 mmol) in 10 mL of water was irradiated for 5 h at 15 °C (λ > 540 nm). The resulting precipitates were filtered and washed with CH_2Cl_2 (5 mL) and acetone (2 mL). The remaining solid afforded **6** (14 mg) in 36% yield based on **1**. From the CH_2Cl_2 washing were obtained **2p** (7 mg, 16%, R_f = 0.49–0.36) and another product **7** (ca. 1 mg, ca. 3%, R_f = 0.75–0.69) by TLC separation (CH_2Cl_2).

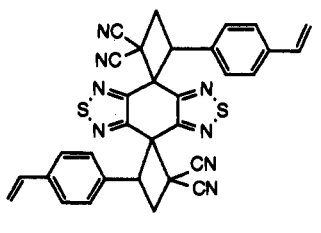

7

The structure of the 2:1 adduct **7** was deduced from the spectral data.[37] The cyclobutane rings in **6** and **7** have the same regiochemistry as that in **2p**, which is indicated by the similarity in ^1H NMR spectra as well as the characteristic fragment peak, $M^+ - CH_2{=}C(CN)_2$, in MS spectra. However, the stereochemistries around the two chiral carbons in **6** and **7** were not determined.

6: pale yellow powder, mp 115–130 °C dec; IR (KBr) 2215 cm^{-1}; ^1H NMR (200 MHz, DMSO-d_6) δ 6.54 (4 H, s), 5.12 (2 H, dd, J = 10.6, 11.9 Hz), 3.82 (2 H, dd, J = 11.9, 11.9 Hz), 3.50 (2 H, dd, J = 10.6, 11.9 Hz); UV (MeCN) λ_{max} = 368 sh (ϵ 18 000), 350 (23 600), 324 (28 000), 290 sh (27 100), 274 (31 200), 222 (29 600) nm; MS m/z (relative intensity) 614 ($M^+ - 2CH_2{=}C(CN)_2$, 67), 613 ($M^+ - 2CH_2{=}C(CN)_2 - 1$, 80), 588 ($M^+ - 2CH_2{=}C(CN)_2 - CN$, 100); HRMS m/z 587.9673 ($M^+ - 2CH_2{=}C(CN)_2 - CN$; calcd for $C_{25}H_6N_{11}S_4$, 587.9690). Anal. Calcd for $C_{34}H_{10}N_{16}S_4{\cdot}4H_2O$: C, 48.45; H, 2.15; N, 26.60. Found: C, 48.44; H, 1.45; N, 27.18.

7: colorless powder, 180–205 °C dec; IR (KBr) 2235 cm^{-1}; ^1H NMR (200 MHz, $CDCl_3$) δ 7.18 (4 H, AA'XX'), 6.72 (4 H, AA'XX'), 6.57 (2 H, dd, J = 11.0, 17.6 Hz), 5.65 (2 H, dd, J = 0.8, 17.6 Hz), 5.22 (2 H, dd, J = 0.8, 11.0 Hz), 5.15 (2 H, dd, J = 8.8, 12.4 Hz), 4.32 (2 H, dd, J = 11.4, 12.4 Hz), 3.27 (2 H, dd, J = 8.8, 11.4 Hz); HRMS m/z 580.1255 (M^+; calcd for $C_{32}H_{20}N_8S_2$, 580.1252), 502.1012 ($M^+ - CH_2{=}C(CN)_2$; calcd for $C_{28}H_{18}N_6S_2$, 502.1034), 424.0786 ($M^+ - 2CH_2{=}C(CN)_2$; calcd for $C_{24}H_{16}N_4S_2$, 424.0816).

CT Excitation Reactions of *o*DV·1 Single Crystals. Single crystals of *o*DV·**1** were obtained as red rods by the vapor diffusion method in MeCN/*n*-hexane. They were sealed piece by piece in glass capillaries for the absolute asymmetric synthesis of **2o**. The samples were irradiated (λ > 540 nm) for 3–5 h in a thermostated bath at four different temperatures (40, 15, –40, and –70 °C). After the photolyses, the resulting yellow crystals were analyzed by HPLC equipped with a SUMICHIRAL OA-2000S column. On eluting with *n*-hexane/CH_2Cl_2/EtOH (100:10:1), the typical retention time was 250 min for (+)-**2o** and 260 min for (–)-**2o**, respectively, with the baseline separation of the peaks. The values of ee shown in the Figure 7 were determined from the ratio of peak areas monitored by the absorbance at 254 nm.

Entrainment of the *o*DV·1 CT Crystal by Seeding. To an oversaturated solution of **1** (15 mg, 0.05 mmol) in *o*DV (2 mL) was added a "seed" single crystal of *o*DV·**1** at 80 °C, and the mixture was allowed to stand at room temperature. The resulting fine red crystals were collected and irradiated for 20 min (λ > 540 nm) to give 4 mg of (–)-**2o** with 11% ee (HPLC). Another solution of **1** in *o*DV was vigorously digested after adding the "seed".[38] The CT crystal began to precipitate in 20 s as a red powder. Similar photolysis afforded 5 mg of (+)-**2o** with 9% ee (HPLC).

Determination of Association Constants (K_{CT}). In the presence of a large excess of donor, K_{CT} values for the EDA complexes of **1** were determined by a spectrophotometric procedure based on the Benesi–Hildebrand relationship[39] in MeCN at 20 °C. In all cases, linear correlations were observed (γ = 0.998–0.999, n = 7–10) indicating a 1:1 molar ratio for the EDA complexes. Molar absorption coefficients (ϵ/$dm^3\ mol^{-1}\ cm^{-1}$) at 460 nm are as follows: *p*DV-**1**, 1400; *m*DV-**1**, 1800; *o*DV-**1**, 1400; ST-**1**, 1100. In these measurements, the concentration of **1** is (1.01–1.07) × 10^{-3} mol dm^{-3} and those of donors are 0.119–1.63 mol dm^{-3}.

X-ray Structural Analyses. All of data collections were performed on an AFC-5R automated four-circle diffractometer equipped with a rotating anode (Mo Kα, λ = 0.709 26 Å),[40] and no absorption correction was applied. No degradation of the crystal by X-ray was ascertained in all cases by repeated monitoring of the three selected reflections every 150 reflections. Details are summarized in Table 2. These structures were solved by direct methods using the RANTAN81 program[41] with some modification. Atomic parameters were refined by the block-diagonal least-squares method by applying anisotropic temperature factors for non-hydrogen atoms. At the final stage, hydrogen atoms were included in the refinement with isotropic temperature factors. All the calculations were carried out on ACOS 2020 and ACOS 3900 computers at Tohoku University by using the applied library program of the UNICS III system.[42] More details of X-ray structural analyses, final atomic coordinates and thermal parameters, bond lengths and angles, structure factors, and thermal ellipsoids with atom numbering systems are deposited as supplementary material.

*o*DV·**1** lost volatile *o*DV gradually on standing so that the single crystal was sealed in a glass capillary during the data collection. All the hydrogen atoms were picked up from the *D*-map and included in the refinement. In order to determine the absolute configuration of this specimen, 19 reflections were selected for the Bijvoet pair measurements with Cu Kα radiation, for which more than 13% of ΔFc will be induced by anomalous scattering [$\Delta Fc = 2\|Fc(hkl)| - |Fc(\bar{h}\bar{k}\bar{l})\|/\{|Fc(hkl)| + |Fc(\bar{h}\bar{k}\bar{l})|\}$]. By comparisons of averaged F_o values for Bijvoet pairs, $[F_o(hkl) + F_o(\bar{h}\bar{k}\bar{l})]$ vs $[F_o(\bar{h}\bar{k}\bar{l}) + F_o(hkl)]$, it was successfully determined that the selected crystal had the absolute configuration as shown in Figures 3a, 4a, and 5a,b. This crystal afforded the (+)-**2o** (HPLC) on irradiation (λ > 540 nm).

A chiral-**2o** crystal suitable for crystallography was obtained after many trials upon irradiation of single crystals of *o*DV·**1** in glass capillaries

(37) Formation of **7** in the solid state could be explained by the further addition of *p*DV to the 1:1 adduct **2p**. This reaction may also proceed via ET because the CT band from *p*DV (E^{ox}, +1.51 V) to **2p** (E^{red}, –0.31 V) would be excited under the present irradiation conditions.

(38) McBride, J. M.; Carter, R. L. *Angew. Chem., Int. Ed. Engl.* **1991**, *30*, 293.

(39) Benesi, H. A.; Hildebrand, J. H. *J. Am. Chem. Soc.* **1960**, *82*, 2134.

(40) Reflection data for *o*DV·**1**, *m*DV·**1**, and chiral-**2o** were measured at the Instrumental Analysis Center for Chemistry, Tohoku University. We thank Dr. Chizuko Kabuto for her generosity in data collection and helpful discussions of crystallographic analyses. Those for *p*DV·**1**, *dl*-**2o**, and $mDV_5{\cdot}I_3$ were collected at the Institute for Molecular Science. The authors also thank the Computer Center, Okazaki National Research Institutes, for the use of a HITAC M-680H computer.

(41) Jia-xing, Y. *Acta Crystallogr. Sect. A* **1981**, *37*, 642; **1983**, *39*, 35.

(42) Sakurai, T.; Kobayashi, K. *Rikagaku Kenkyusho Hokoku* **1979**, *55*, 69.

at 40 °C for 4 h ($\lambda > 540$ nm). Several crystals suffered cracking of the specimens especially when the photoirradiations were conducted at lower temperatures. This crystal is isomorphous to *o*DV·**1** with adopting the $P2_1$ space group. The absolute configuration was not determined for this crystal and was shown as (*R*)-**2o** for easy comparisons of the coordinates and structures (Figures 3b, 4b, and 5c) with those of *o*DV·**1**. Because the value of ee is expected to be ca. 60% for this crystal, there will be molecules of **2o** having the (*S*)-configuration in 20% proportion. However, the *D*-synthesis after the refinement afforded only a small residual electron density (0.58 e/Å^3), so that we could not determine the positions of disordered atoms corresponding to (*S*)-**2o**. Because the atomic positions were refined without involving the (*S*)-**2o** molecules, some atoms possess very large thermal parameters especially along the c^* axis (U_{33}). Hydrogen atoms were not included in the refinement.

dl-**2o** was obtained on recrystallization of a racemic mixture of the as-prepared adduct 2o from CH_2Cl_2/*n*-hexane. This crystal adopts the centrosymmetric space group $P2_1/n$ (racemic compound), and the packing arrangement is quite different from that of chiral-**2o**. In the crystal, the two molecules are connected by S(1)--N(5)≡C(9) interaction (3.36 Å) to form a centrosymmetric dyad, and no further S--N≡C contacts were observed between the dyads. All the hydrogen atoms were appeared on the *D*-map and included in the refinement.

*m*DV·**1** (phase A) is efflorescent like *o*DV·**1** and was also sealed in a glass capillary for the data collection. This crystal was formed along with *m*DV$_5$·**1**$_3$ (phase B) in the same batch; however, two phases were easily discriminated by their appearance and cell parameters.[21] Most of the hydrogen atoms were picked up from the *D*-map and included in the refinement with others calculated geometrically.

*p*DV·**1** crystallizes in the centrosymmetric space group $P\bar{1}$, and each molecule of *p*DV and **1** lies on an inversion center. In contrast to other CT crystals of DV isomers, the vinyl groups in *p*DV are positionally disordered and adopt the three different positions as C(21)—C(241)=C(251), C(21)—C(241)=C(252), and C(21)—C(242)=C(251). The latter two vinyl positions could be almost superimposed by rotation of the benzene nucleus by ca. 40°, suggesting that the ring carbons were also positionally disordered. However, those atoms were refined as located at the center of gravity without dividing into two atomic positions, thus giving such unusual bond angles around C(21) as 93(1)° for C(23′)–C(21)–C(241) or 147(1)° for C(22)–C(21)–C(242).

Powder X-ray Analyses. Water suspensions (10 mL) of *o*DV·**1** (120 mg, 0.27 mmol) were irradiated separately (2-kW xenon, $\lambda > 540$ nm, 15 °C) for 5 and 15 min, and the resulting precipitate was analyzed by the XRD technique[43] (Cu Kα, 40 kV, 20 mA, 2° min^{-1}) along with *o*DV·**1** and *dl*-**2o**. The conversions of the CT crystal were determined to be 43% and 84%, respectively, by the TLC separation of **2o** (CH_2Cl_2). Similarly the reaction of *m*DV·**1** was followed by XRD (Cu Kα, 40 kV, 50 mA, 2° min^{-1}) as shown in Figure 10. The isolated yields of **2m** were 6%, 16%, 20%, 28%, and 30%, respectively, when water suspensions of *m*DV·**1** (120 mg, 0.27 mmol) were irradiated separately for 1, 3, 5, 7, and 10 h ($\lambda > 540$ nm) at 15 °C.

Acknowledgment. Financial support (to T.S.) by the CIBA-GEIGY Foundation (Japan) for the Promotion of Science and by the Shorai Foundation for Science and Technology is gratefully acknowledged. This work was also supported by the Joint Studies Program (1991–1992) of the Institute for Molecular Science and by a Grant-in-Aid (No. 03403005 to T.M.) from the Ministry of Education, Science and Culture, Japan.

Supplementary Material Available: Text describing details of X-ray structural analyses, figures showing thermal ellipsoids with atom numbering systems, and tables listing atomic and thermal parameters and bond lengths and angles for *o*DV·**1**, chiral-**2o**, *dl*-**2o**, *m*DV·**1**, *p*DV·**1**, and *m*DV$_5$·**1**$_3$ (38 pages); listings of observed and calculated structure factors (42 pages). This material is contained in many libraries on microfiche, immediately follows this article in the microfilm version of the journal, and can be ordered from the ACS; see any current masthead page for ordering information.

(43) The authors thank Prof. Mamoru Shimoi, The University of Tokyo, and Mr. Takaaki Hanaoka, National Institute of Materials and Chemical Research, for their help in the powder X-ray analyses.